PHYSICAL REVIEW E

STATISTICAL PHYSICS, PLASMAS, FLUIDS, AND RELATED INTERDISCIPLINARY TOPICS

THIRD SERIES, VOLUME 60, NUMBER 4 PART B OCTOBER 1999

ARTICLES

Dynamics of chevron structure formation. II. Permeation-dominated phenomena

A. N. Shalaginov,* L. D. Hazelwood, and T. J. Sluckin

Southampton Liquid Crystal Institute and Faculty of Mathematical Studies, University of Southampton, Southampton SO17 1BJ, United Kingdom

(Received 28 January 1999)

This paper continues a study of the dynamics of chevron formation in smectic-*A* liquid crystals in samples with boundary conditions apparently favoring the bookshelf structure, with uniform layers perpendicular to the sample cell plane. The chevron structure that arises when the sample is cooled results from the mismatch between preferred bulk and surface layer thicknesses. In a previous paper we considered relaxation driven by the strong coupling between layer deformation and fluid flow. In this paper we discuss the alternative scenario in which boundary conditions suppress this coupling. Layer deformation now occurs by layer relaxation in the absence of fluid flow. This process is extremely slow and is governed by the nonlinear Fisher-Kolmogorov equation. Chevrons do form under some circumstances, but the process is irregular, and quasimetastable jagged multi-edged multi-tip-like structures can occur on intermediate time scales for suitable layer strains. In the absence of surface layer pinning, layer slippage occurs at the surfaces. We also examine the possibility that deformation may occur through a wave of invasion destroying the bookshelf region.
[S1063-651X(99)10509-9]

PACS number(s): 61.30.Cz, 42.79.Kr, 64.70.Md, 83.70.Jr

I. INTRODUCTION

This paper is the second of two studies of the dynamics of chevron formation in smectic-*A* liquid crystals. We shall refer to the first study [1] as I. The chevrons are the result of layer buckling that occurs when the liquid crystal is placed in a sample with homogeneous boundary conditions that one would naively expect to favor a so-called bookshelf geometry, with uniform layers perpendicular to the sample plane. There is now good evidence that the chevrons occur as a result of mismatch between bulk and surface layer thicknesses.

We show the chevron geometry in Fig. 1. We refer the reader to other papers for a more detailed experimental and theoretical background [2–7]. We note here only that there are a considerable number of experiments, most notably in the related smectic-*C* phase, and that theoretical work on the statics seems to confirm the picture presented above.

The consensus is that the chevron structure is the consequence of the mismatch between the natural smectic reciprocal layer spacing q_B and the reciprocal layer spacing q imposed by the surface interaction. We can define the strain $\epsilon = 1 - q/q_B$. How the strain arises is more of a mystery. In the simplest hypothesis, it follows from layer pinning at the boundaries while at the same time q_B and q change differently with temperature. More elaborate hypotheses do not demand this postulate and ascribe the layer mismatch to vastly differing time scales of surface and bulk relaxation. In any event, in many circumstances the chevrons do form, so long as the strain is greater than a critical strain

$$\epsilon_c = 4\pi^2 K/BL^2,$$

where K and B are the smectic bending and compression elastic coefficients and L is the cell thickness. In previous work we have found it useful to nondimensionalize this strain in terms of the so-called chevron number [6], $\sigma = \epsilon/\epsilon_c$.

In I we developed a formalism to account for the chevron structure dynamics for a quenched system for which the bookshelf structure is no longer stable. In this picture, the chevron structure develops from thermal fluctuations following spontaneous symmetry breaking. The resulting set of equations involves an equation of fluid motion and a relax-

*Permanent address: Department of Physics, University of St. Petersburg, St. Petersburg 198904, Russia.

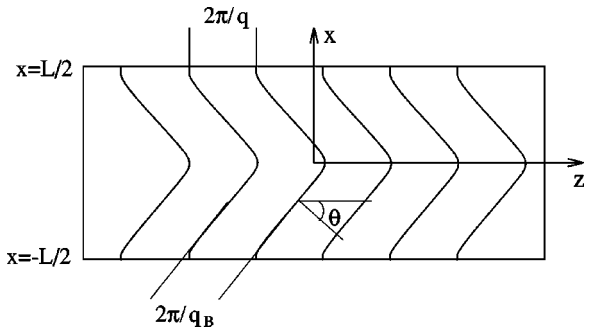

FIG. 1. Picture of the chevron structure, with cell of width L, and showing natural layer wave number q_B, surface-imposed wave number q, conventions for x and z axes, and layer angle θ.

ation equation for the smectic order parameter in the moving system. These equations are coupled, with the forcing terms in the order parameter equation and in the equation of motion proportional to each other. It turns out that, if it is possible, the layer displacement of the chevron primarily occurs in the fluid motion. The process whereby the layers move with respect to the fluid, a process known as *permeation* [8] in the liquid crystal literature, is some eight orders of magnitude slower than the fluid-induced motion. The coupling between layer and fluid motion shortens the time necessary for chevron structure to develop from weeks to milliseconds.

In this paper we continue the study which we began in I, by considering a situation in which the boundary conditions at the ends of the cell are such as to suppress almost entirely fluid motion. We may suppose that whereas in I the fluid was free to slosh around in the plane of the cell, in contrast now the liquid crystal is enclosed by fixed boundaries at the edge of the cell. The result is to reduce the number of equations, for now we must consider the smectic order parameter (in this case the layer displacement) relaxation alone. In principle, this appears to be a simplification. In practice, however, our previous study benefited from the existence of a small parameter $\delta_2=\tau_p/\tau_v\sim 10^{-8}$, where τ_v,τ_p are, respectively, the characteristic viscous (fluid) and permeation relaxation times. This small parameter rendered some dangerous nonlinear terms irrelevant in our previous paper, but these terms return with a vengeance to haunt us in this study.

In I we found that the development of the chevron was rather straightforward. The chevron tip developed almost according to a universal law, when suitable normalizations and time scales were considered. The chevron tip followed a monotonic tanh-like curve as a function of time.

Once fluid flow is suppressed, however, apart from the necessary dramatic slowing down of the relaxation process, this quasi-universality no longer holds. We shall find that under some circumstances there will be surface layer slippage, leading to uniform tilted layers. If this is forbidden, chevrons do form. However, they form in an irregular way, with the intermediate states—depending on the value of σ—sometimes developing more than one layer bend before finally settling down to the uniform chevron state. In addition we shall see that the free energy relaxation involves long periods of stasis, with some periods of dramatic rapid collapse. We shall also see that one plausible scenario is that the chevron creation takes place through an invasion process, rather than through homogeneous creation.

The plan of the paper is as follows. In Sec. II we give the necessary background to the equilibrium chevron structure. Then in Sec. III we provide a very brief summary of paper I and exhibit the equations that govern our study. We then present the results of a study of homogeneous nucleation of the chevron phase. Then in Sec. V we present some calculations on the domain wall motion model of the formation of the chevron phase. Finally, in Sec. VI we combine these studies, together with paper I, and draw some brief conclusions.

II. STATICS

A. Elastic energy

We recall some basic notions from I. The smectic layer structure is described by a phase function $W(\mathbf{r},t)$ [6], so that a layer is a surface $W(\mathbf{r},t)=\text{const}$. The director $\mathbf{n}$, which points along the average local orientation of the molecules, is a fast variable, with relaxation time $\sim 10^{-7}$ s [10]. On the time scales considered in this paper, the elastic energy can be expressed in terms of W only. The energy density is given by [9]

$$f(\mathbf{r})=\frac{1}{8}B[q_B^{-2}(\nabla W)^2-1]^2+\frac{1}{2}Kq_B^{-2}(\nabla^2 W)^2. \qquad (1)$$

We perform calculations in a Cartesian coordinate system $\mathbf{r}=(x,y,z)$, with conventions shown in Fig. 1. The Sm-A liquid crystal is confined between two plates located at $x=-L/2$ and $x=L/2$. The layers are stacked along the z direction because the boundary conditions impose $\hat{\mathbf{n}}=\hat{\mathbf{z}}$ at the surfaces. We take the system to be uniform along the y axis, so that physical quantities are functions of x,z only.

The absolute free-energy minimum in an unconfined but oriented system occurs for $W=q_B(z-z_0)$, which corresponds to a stack of smectic layers perpendicular to the z axis. The quantity q_Bz_0 is an arbitrary phase factor. In the bookshelf structure, q_B is replaced by the surface-imposed reciprocal layer spacing q. Deviations from the bookshelf structure can be described by

$$W=q[z-u(\mathbf{r})], \qquad (2)$$

where u is the layer displacement.

The critical strain ϵ_c is a small parameter. For a cell with $L=2\times 10^{-3}$ cm and $\lambda=\sqrt{K/B}\approx 3\times 10^{-7}$ cm, we find $\epsilon_c\approx 10^{-6}$. The strain is defined by the layer mismatch,

$$\epsilon=1-\frac{q}{q_B}, \qquad (3)$$

which is the fractional difference between the natural and imposed layer periodicities. It will be useful to note that $1-q^2/q_B^2\approx 2\epsilon$. Substituting Eq. (2) into Eq. (1) while truncating at lowest order in ϵ, u_x, and u_z yields the following re-expression of the free-energy functional in terms of the local layer displacements:

$$F=\frac{1}{2}\int d^3r\left[B\left(\frac{1}{2}u_x^2-u_z-\epsilon\right)^2+K(u_{xx})^2\right]. \qquad (4)$$

We have dropped terms linear in u_{zz} and u_z^2, which are higher order in the small quantity u.

This is the free energy we have used in I, apart from allowing inhomogeneities in the z direction not considered there. Setting $\epsilon=0$ gives rise to the expression for the elastic free energy with a nonlinear term that guarantees invariance with respect to rotations [8]. Furthermore, putting $u_z=0$ and $\theta=u_x$ in Eq. (4) yields the Limat-Prost model [5] of the chevron structure.

Equilibria of the system are defined by

$$\frac{\delta F}{\delta u}=0 \tag{5}$$

or, equivalently,

$$\left(\frac{\partial}{\partial z}-\frac{\partial}{\partial x}u_x\right)\left(\frac{1}{2}u_x^2-u_z-\epsilon\right)+\frac{L^2}{4\pi^2}\epsilon_c u_{xxxx}=0. \tag{6}$$

We briefly recall from I the equilibrium structure, for which $u_z=0$. Elsewhere [5,6], this has been considered in terms of the layer tilt angle θ, with $u_x=\tan\theta\approx\theta$. The approximation is true for small tilts, which in practice is always the case. Here we reformulate the problem in terms of the displacement u. In principle, the energy is minimized by a displacement field $u(x)=\sqrt{2\epsilon}x$. This, however, requires slipping of the smectic layers at the bounding plates. This seldom occurs, because the boundary conditions seem to pin the layers at the interfaces:

$$u(\pm L/2)=0. \tag{7}$$

In addition, it appears [5,6] that it is reasonable to impose infinite anchoring:

$$u_x(\pm L/2)=\theta(\pm L/2)=0. \tag{8}$$

The interplay between the bulk elastic energy and boundary conditions yields the chevron structure. There are two wide regions in which the layers are flat, but tilted so as to have the correct packing. In the middle of the cell there is an interphase region of thickness $2\lambda/\sqrt{2\epsilon}$ [5]. There are also two narrow high curvature regions at the cell walls, whose thickness depends on the surface anchoring, and which disappear as the anchoring strength vanishes.

This analysis [5,6] was actually carried out in terms of θ and the nonslip boundary conditions were satisfied by restricting $\theta(x)$ to be an odd function. This procedure is convenient for the study of stable states, but fails for dynamics. We thus return to a study of the governing differential equation in terms of displacement u. However, we emphasize that this is a *fourth-order* equation in u, rather than a *second-order* equation in θ. The significance of this remark will become clear later in our study.

B. Near-critical strain: Statics

The Euler-Lagrange equation (6) can in general be solved only numerically. However, insight can be gained by detailed analysis for strains just above the critical strain: $\epsilon/\epsilon_c \ll 1$. We first briefly recall the analysis for a system uniform in the z direction for this regime, and then pass to the more interesting nonuniform case.

In the uniform case Eq. (6) can be linearized to yield

$$\epsilon u_{xx}+\frac{L^2}{4\pi^2}\epsilon_c u_{xxxx}=0. \tag{9}$$

The solution of this equation satisfying the boundary conditions is

$$u(x)=\frac{L}{2\pi}A_1\left(1+\cos\frac{2\pi x}{L}\right). \tag{10}$$

This is the principal mode in a Fourier expansion of the full chevron deformation.

The amplitude of A_1 is then determined by taking the weakly nonlinear limit of Eq. (6), or by substituting the variational form (10) into the functional (4). In either case, this yields a Ginzburg-Landau equation for A_1:

$$\frac{3}{8}A_1^3+A_1(\epsilon_c-\epsilon)=0, \tag{11}$$

with solution

$$A_1=\pm 2\sqrt{\frac{2(\epsilon-\epsilon_c)}{3}}, \tag{12}$$

where the sign imprecision corresponds to the two equivalent opposite symmetry deformations. This analysis corresponds to Sec. IV B and Eq. (58) of I.

We now examine the behavior of this deformation close to the end of the cell at $z=0$, where we may suppose that the boundary conditions compel the layers to be *exactly* bookshelf, and thus with deformation $A_1=0$. The deformation in this regime can now be expressed in terms of the principal mode,

$$u(x,z)=\frac{L}{2\pi}A(z)\left(1+\cos\frac{2\pi x}{L}\right), \tag{13}$$

where the amplitude of the deformation is described by the function

$$A(z)=A_1 g(z), \tag{14}$$

and its spatial dependence by $g(z)$ with $g(0)=0$ (i.e., no deformation) and $g(\infty)=1$ (i.e., full deformation).

The behavior of the deformation is now described by the differential equation,

$$\xi_p^2\frac{\partial^2 g}{\partial z^2}+g-g^3=0, \tag{15}$$

which generalizes Eq. (11) to the nonuniform cell. The penetration depth ξ_p is defined by

$$\xi_p=\frac{L}{2\pi}\sqrt{\frac{3}{\epsilon-\epsilon_c}}. \tag{16}$$

The solution to Eq. (15) satisfying these conditions is given by

$$g(z)=\tanh\left(\frac{z}{\sqrt{2}\xi_p}\right). \tag{17}$$

The chevron structure develops from the wall over a characteristic length $\sqrt{2}\xi_p$. We shall show later in this paper that the penetration depth ξ_p also plays a role in moving fronts between deformed and undeformed regions.

III. DYNAMICS: HOMOGENEOUS NUCLEATION

A. Basic equations

In I we have discussed in detail the dynamical equations that govern the chevron formation. These equations involve Navier-Stokes equations that govern fluid motion, and a time-dependent Ginzburg-Landau equation governing permeation. By far the dominant effect of layer mismatch arises in the Navier-Stokes equation, and the effect of the Ginzburg-Landau equation is a negligible long-time relaxation correction.

We now suppose the mass flow to be strictly forbidden as a result of the edge conditions. As a result, only one of the full set of hydrodynamic equations is relevant,

$$\frac{\partial u}{\partial t}-v_3=\boldsymbol{\nabla}\cdot\mathbf{J}, \tag{18}$$

with v_3 the velocity component in the z direction and $\mathbf{J}$ a phase flux term:

$$J_k=\lambda_p\frac{\delta F}{\delta\nabla_k u}. \tag{19}$$

The quantity λ_p is the usual permeation constant of Sm-*A* hydrodynamics [8], which relates the layer flux through a stationary medium to the relevant thermodynamic force. In a more general case, this equation could also include a term proportional to $\nabla \boldsymbol{T}$, but in this paper we shall assume for simplicity that the temperature is constant throughout the cell. Equation (18) is just a time-dependent Ginzburg-Landau (TDGL) equation for the conserved variable u.

We now make some remarks about the zero-mass-flow condition. For homogeneous chevron nucleation, v_3 is uniform in the z direction by definition. This condition, combined with the incompressibility condition $\boldsymbol{\nabla}\cdot\mathbf{v}=0$, forces v_1 to be uniform in the x direction. But as the fluid is fixed at each face of the cell, we necessarily must have $v_1=0$. If the edges of the cell are fixed, then homogeneous nucleation demands $v_3=0$. Thus in this case there can be no fluid motion at all. The situation can, in principle, be complicated in the case of inhomogeneous nucleation, which we shall discuss in the next section, but even here it turns out that fluid motion can be neglected.

Setting $v_i=0$ we obtain the time-dependent Ginzburg-Landau equation,

$$u_t=-\lambda_p\frac{\delta F}{\delta u}, \tag{20}$$

where F is defined by Eq. (4). The functional derivative is

$$\begin{aligned}\frac{\delta F}{\delta u}&=-\frac{\partial}{\partial x}\frac{\partial F}{\partial u_x}-\frac{\partial}{\partial z}\frac{\partial F}{\partial u_z}+\frac{\partial^2}{\partial x^2}\frac{\partial F}{\partial u_{xx}}\\&=-\frac{\partial}{\partial x}\left[B\left(\frac{1}{2}u_x^2-u_z-\epsilon\right)u_x-Ku_{xxx}\right]\\&\quad+\frac{\partial}{\partial z}\left[B\left(\frac{1}{2}u_x^2-u_z\right)\right].\end{aligned} \tag{21}$$

In the homogeneous nucleation case this reduces to:

$$u_t=\lambda_p\frac{\partial}{\partial x}\left[B\left(\frac{1}{2}u_x^2-\epsilon\right)u_x-Ku_{xxx}\right]. \tag{22}$$

We remark as a footnote to this discussion that this TDGL guarantees positive energy dissipation, as the following argument demonstrates. Using Eq. (20), the energy dissipation is given by

$$\frac{dF}{dt}=\int d^3r\frac{\delta F}{\delta u}u_t=-\lambda_p^{-1}\int d^3r u_t^2\leqslant 0. \tag{23}$$

Thus the free energy of the system always decreases until a local or global minimum is reached.

Physically, Eq. (22) describes how the molecules rearrange themselves, forming new layers during the formation of a chevron structure in a cell with closed ends. In this process the smectic layers can be thought of as moving through the fluid. The process is expected to be very slow because the permeation constant is typically small.

B. Time scale and nondimensionalization

We first estimate the relevant time scale. To do this, we linearize the governing equation (22),

$$u_t=-\lambda_p(\epsilon Bu_{xx}+Ku_{xxxx}), \tag{24}$$

and take $\partial_x\sim 1/L$. If $\epsilon<\epsilon_c$ there is no chevron; otherwise we take the smaller of two possible times, which involves the second term, replacing K by $\sim\epsilon_c BL^2$. Thus we derive the permeation time scale first discussed in the Introduction:

$$\tau_p=\frac{L^2}{\epsilon_c B\lambda_p}=\frac{L^4}{4\pi^2\lambda_p K}. \tag{25}$$

Taking $\epsilon=10^{-5}$, $L=10^{-3}$ cm and $B\lambda_p=10^{-5}$ cm^2 s^{-1} [8], we find the time scale of 10^4 s.

We thus nondimensionalize the time variable by dividing by τ_p. We now introduce dimensionless parameters:

$$\tilde{x}=\frac{x}{L}, \tag{26a}$$

$$\tilde{t}=\frac{t}{\tau_p}, \tag{26b}$$

$$U(\tilde{x},\tilde{t})=\frac{u(x,t)}{L\sqrt{2\epsilon_c}}, \tag{26c}$$

$$\vartheta(\tilde{x},\tilde{t})=\frac{\partial U(\tilde{x},\tilde{t})}{\partial\tilde{x}}=\frac{\theta(x,t)}{\sqrt{2\epsilon_c}}. \tag{26d}$$

Equation (20) can be simply reexpressed in this new notation,

$$U_{\tilde{t}}=\frac{\partial}{\partial\tilde{x}}\frac{\delta\mathcal{F}}{\delta\vartheta}, \tag{27}$$

where now the dimensionless free energy and its functional derivative with respect to scaled angle are,

$$\mathcal{F}=\frac{1}{2}\int_{-1/2}^{1/2}d\tilde{x}\left[\frac{1}{2}(\vartheta^2-\sigma)^2+\frac{1}{4\pi^2}\vartheta_{\tilde{x}}^2\right], \tag{28a}$$

$$\frac{\delta\mathcal{F}}{\delta\vartheta}=\vartheta(\vartheta^2-\sigma)-\frac{1}{4\pi^2}\vartheta_{\tilde{x}\tilde{x}}, \tag{28b}$$

where $\sigma=\epsilon/\epsilon_c$ is the chevron number discussed in the introduction [6].

The displacement U is a natural hydrodynamic variable. Nevertheless, as in I we find it more useful to write down the dynamical equation in terms of the scaled angular variable ϑ:

$$\vartheta_{\tilde{t}}=\frac{\partial^2}{\partial\tilde{x}^2}\frac{\delta\mathcal{F}}{\delta\vartheta}=(3\vartheta^2-\sigma)\vartheta_{\tilde{x}\tilde{x}}+6\vartheta\vartheta_{\tilde{x}}^2-\frac{1}{4\pi^2}\vartheta_{\tilde{x}\tilde{x}\tilde{x}\tilde{x}}. \tag{29}$$

However, unfortunately not all solutions of Eq. (29) satisfying the boundary condition Eq. (8) $\vartheta(\pm1/2)=0$ are valid. The change in variable from U to ϑ has caused the information about slipping at the interfaces to be lost — equivalently, the information $U(\pm1/2)=0$ has not been used. This information can be retrieved by applying the nonlocal condition

$$\int_{-1/2}^{1/2}d\tilde{x}\,\vartheta(\tilde{x},\tilde{t})=0. \tag{30}$$

This integral condition presents formidable technical mathematical difficulties which in general outweigh the advantages of rephrasing the problem in terms of ϑ. Fortunately, however, in this case the principal mode $\vartheta\sim\sin(2\pi\tilde{x})$ responsible for the formation of the chevron structure is an odd function in $\tilde{x}$. In addition, Eq. (29) contains only terms odd in ϑ.

Thus any solution $\vartheta(\tilde{x},\tilde{t})$ which is an odd function at $\tilde{t}=0$ remains odd for all times and then satisfies Eq. (30) automatically. The descriptions in terms of U and ϑ are equivalent so long as we confine our discussion to odd ϑ and even U.

C. Spectral analysis

The governing equation (29) is a fourth-order nonlinear differential equation. Fourth-order differential equations present notorious stability problems within finite difference schemes. As a result, we have used a spectral method, which we now describe briefly.

The manifold of solutions $\vartheta(\tilde{x})$ is explicitly restricted to functions odd in $\tilde{x}$. This choice guarantees that $U(\tilde{x},\tilde{t})$ satisfies layer nonslip conditions. Then we recall that an odd function satisfying the boundary condition equation (8) $\vartheta(\pm1/2)=0$ can be expanded in a sine Fourier series:

$$\vartheta(\tilde{x},\tilde{t})=\sum_{n=1}^{\infty}\mathcal{A}_n(\tilde{t})\sin(2\pi n\tilde{x}). \tag{31}$$

The governing equation (29) is a *partial* differential equation in space and time. Using standard projection methods, it can now be rewritten as a set of nonlinear first-order *ordinary* differential equations governing the time evolution of the Fourier coefficients $\mathcal{A}_n(\tilde{t})$.

Following some straightforward but (extremely!) tedious algebra which we omit, we obtain

$$\frac{d\mathcal{A}_n}{d\tilde{t}}=4\pi^2n^2(\sigma-n^2)\mathcal{A}_n+2\sum_{k,l,m=1}^{\infty}\Pi_{nklm}\mathcal{A}_k\mathcal{A}_l\mathcal{A}_m, \tag{32}$$

where the coefficients Π_{nklm} are defined as

$$\Pi_{nklm}=-4\pi^2n^2\int_{-1/2}^{1/2}d\tilde{x}\sin(2\pi n\tilde{x})\sin(2\pi k\tilde{x})\times\sin(2\pi l\tilde{x})\sin(2\pi m\tilde{x}). \tag{33}$$

In the weak chevron limit, only the $\mathcal{A}_1$ equation is relevant, and other modes can be ignored. The permeation-driven chevron development will turn out to be qualitatively exactly the same as in the hydrodynamically driven case discussed in I. Only the time scale is slower (by a factor of 10^8). In this regime other modes decay. Because even $\mathcal{A}_1$ remains small, the nonlinear terms in the equations for $\mathcal{A}_n, n\geq2$ remain unimportant. As a result, these equations remain essentially linear and independent.

At early times, soon after the bookshelf structure has been quenched into an unstable state, the linear limit of Eq. (32) is sufficient for *all* values of σ. The equations are independent. For low enough n the amplitudes $\mathcal{A}_n$ grow, and for high n they decrease, in each case with its own characteristic time. However, for these higher values of σ, the nonlinear terms eventually lead to mode coupling.

This interaction between the harmonics can only be neglected for very weak chevrons ($|(\sigma-1)|\ll1$), and at early times. Otherwise it must be taken into consideration. In principle, there is an infinite set of nonlinear ordinary differential equations. In practice, it is necessary to truncate this set of equations at some harmonic N. We can estimate N by noting that the nth harmonic resolves length scales $\Delta\tilde{x}_n\sim(2\pi n)^{-1}$. However, from Eq. (28a) we can see that the characteristic length over which changes occur in the static chevron is $\Delta\tilde{\xi}\sim(2\pi\sqrt{\sigma})^{-1}$. We shall not require values of n in the harmonic expansion that cause changes on length scales shorter than $\tilde{\xi}$. Putting $\Delta\tilde{\xi}\sim\Delta\tilde{x}_N$ yields $N\sim\sigma^{1/2}$.

D. Early-time analysis

At early times, soon after the bookshelf structure has been quenched into an unstable state, ϑ is small and the evolution may be described by the linearized permeation equation. The evolution of the nth harmonic is described by

$$\frac{\partial \mathcal{A}_n}{\partial \tilde{t}} = 4\pi^2 n^2(\sigma - n^2)\mathcal{A}_n = \gamma_n \mathcal{A}_n . \tag{34}$$

These equations display interesting features and may be compared with the analogous case discussed in I. In that case mass flow is permitted; the n^2 contribution to γ_n governs the dominance of the modes with increasing σ. This differs dramatically from the evolution of the equivalent modes in I. In that case the factor of $4\pi^2 n^2$ is absent.

The consequence of this difference is as follows. If, as in I, mass flow is permitted, the fundamental harmonic is dominant at early times for *all* σ, in the sense that the growth rate of the fundamental mode is always larger than those of the other modes. In the case discussed in this paper, this is no longer true. Now γ_n has a maximum around $n = \sqrt{\sigma/2}$. The dominant mode is that for which, roughly speaking, integer n is close to this optimal value and γ_n is largest.

Specifically, the nth mode becomes dominant when it just begins to grow faster than the $(n-1)$th mode. This will occur when

$$\gamma_n = \gamma_{n-1} \tag{35}$$

or, equivalently,

$$n^2(\sigma - n^2) = (n-1)^2[\sigma - (n-1)^2]. \tag{36}$$

Thus

$$\sigma[n^2 - (n-1)^2] = [n^4 - (n-1)^4], \tag{37}$$

or

$$\sigma_n = n^2 + (n-1)^2 = 2n^2 - 2n + 1. \tag{38}$$

This yields the following results for σ_n for low n:

σ_n	1	5	13	25
n	1	2	3	4

(39)

The $\sigma_n = 1$ case marks the critical value for any chevron formation. For deeper quenches n is larger, and then for $\sigma_n \leqslant \sigma < \sigma_{n+1}$, the nth mode dominates. In this case the system is likely initially to develop spatial modulations in ϑ with wave number $2\pi n$.

E. Fundamental mode behavior over long times

To look at the long-time limit we start by considering the weak chevron case. As discussed above, in this regime only the $\mathcal{A}_1$ sine-wave term in the expansion (31) is relevant. This limit obtains in the near critical region $\sigma \geqslant 1$ whose statics were discussed in Sec. II B. The amplitude $\mathcal{A}_1$ then corresponds to the amplitude A_1. Equation (32) then reduces to the familiar time-dependent Ginzburg-Landau form:

$$\frac{d\mathcal{A}_1}{d\tilde{t}} = 4\pi^2\left[(\sigma - 1)\mathcal{A}_1 - \frac{3}{4}\mathcal{A}_1^3\right]. \tag{40}$$

This mode evolves continuously and monotonically from an initial fluctuation up to $\mathcal{A}_1(\infty) = 2\sqrt{(\sigma-1)/3}$. In the limit $(\sigma - 1) \ll 1$ only this mode is important. Equation (40) has sets of solutions of the form

$$\mathcal{A}_1(\tilde{t}) = 2\left(\frac{(\sigma-1)}{3}\right)^{1/2}\{1 + \exp[-8\pi^2(\sigma-1)(\tilde{t} - \tilde{t}_0)]\}^{-1/2}. \tag{41}$$

Note that $\tilde{t}_0$ is the time at which the amplitude reaches half its final value, rather than the time at which the time evolution starts. At the initial time the amplitude is very small, and this corresponds to some $\tilde{t}_1 \ll \tilde{t}_0$. The size of the initial fluctuation affects $\tilde{t}_1$, but the subsequent development is otherwise insensitive to it.

This is close to a tanh-like form, starting close to 0, increasing steeply around $\tilde{t} = \tilde{t}_0$, and then stabilizing at the final equilibrium value. Final behavior is exponential with a characteristic formation time $\tau_p/[8\pi^2(\sigma-1)]$, which diverges at the critical point $\sigma = 1$. The characteristic time for initial growth is faster than this by a factor of 2.

The weak chevron displacement has the cosine form given by Eq. (10). As σ is increased, however, the equilibrium chevron displacement sharpens up and approaches its characteristic V shape with small rounded healing regions close to the walls and at the chevron tip. In this regime the time evolution is analogous to the hydrodynamical case discussed in I, although on a dramatically longer time scale. The spatial structure of the dominant mode is, however, just as in I. However, as we have seen in the last section, as σ passes first through the threshold of σ_2 and then past higher σ_n, the behavior changes. It is to this evolution behavior we turn in the next section.

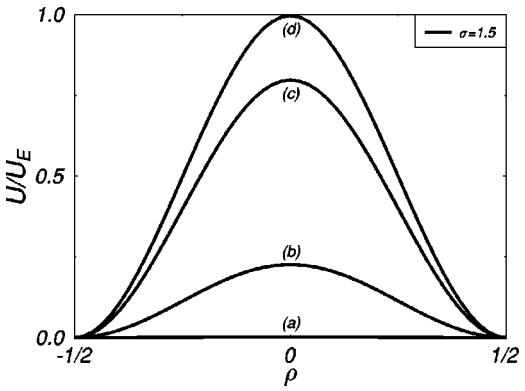

FIG. 2. Time development of the $\sigma = 1.5$ chevron, showing the monotonic time dependence of displacement U. Time (a) is the initial fluctuation. Times (b) through (d) exhibit illustrative snapshots at consecutive later times.

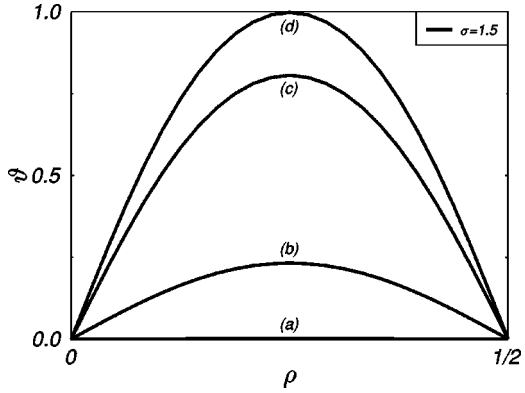

FIG. 3. Time development of the $\sigma=1.5$ chevron, showing the monotonic time dependence of nondimensionalized angle ϑ over half of the cell. The other half of the cell is a mirror image of this. Graph legend as in Fig. 2.

F. Long-time behavior at higher chevron number

For $\sigma \geqslant \sigma_2$ the time evolution changes qualitatively, as a result of the dominance of higher harmonics. We have now solved the set of first order spectral differential equations numerically using the fourth-order Runge-Kutta method [11]. The number of modes N was chosen so that the values of $\mathcal{A}_n$ were insensitive to the adding of extra modes. In addition, A_{N+1} is negligible. The equilibrium solution can be further checked by observing that in this case the quantity

$$I(x)=\frac{1}{4\pi^2}\vartheta_x(x)^2-\frac{1}{2}\left(\vartheta(x)^2-\sigma\right)^2$$

remains essentially constant. This quantity is analytically exactly constant in the static case.

The details of the numerical results are extremely sensitive to the initial conditions and the quench severity. In an infinite system with a random initial fluctuation, the system would develop all modulation lengths $2\pi/n$ consistent with $\sigma \geqslant n^2$, with the fastest-growing mode at $n^2 \approx \sigma/2$. Which mode dominates the intermediate time behavior depends sensitively on how the initial amplitudes of individual modes compete with their relative rates of growth.

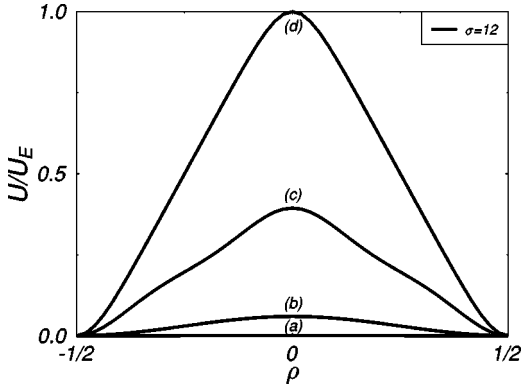

FIG. 4. Time development of the $\sigma=12$ chevron, showing the time dependence of displacement U. Times (a) through (d) represent consecutive snapshots as in Fig. 2. Graph legend as in previous figures.

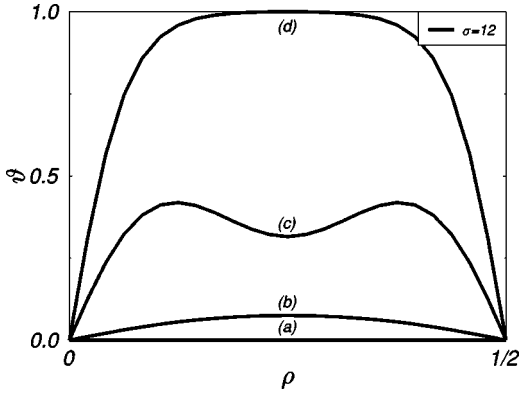

FIG. 5. Time development of the $\sigma=12$ chevron, showing the time dependence of nondimensionalized angle ϑ over half of the cell. The other half of the cell is a mirror image of this. Graph legend as in previous figures. Note the transient development of the $n=2$ mode.

In our calculations we start with an initial fluctuation of $\vartheta_1=10^{-3}$ in the fundamental mode, and this appears to restrict the solution manifold. By this we mean that we observe dominance by modes with lower n than the linear early-time analysis might predict. With no initial fluctuation at all there will be no subsequent time evolution. An initial small fluctuation in the fundamental mode is sufficient to induce subsequent evolution in higher n modes through the nonlinear terms. These induced modes then grow, and at sufficiently high n grow faster than the fundamental mode. However, the extent to which faster mode growth can compensate for lack of initial mode amplitude depends very crucially on the magnitude of the initial conditions, rounding errors and so on.

In the figures we show how the time development changes as σ is increased. In Figs. 2 and 3 we show the evolution of the scaled displacement U and the nondimensionalized angle ϑ over the whole width of the cell, for $\sigma=1.5$. This lies well inside the region where the growth of the fundamental mode is fastest. Indeed, here the relatively low value of σ means that the shape of the equilibrium chevron is not well developed, and ϑ does not closely approach its natural values of ± 1 except at isolated points. We see that, as for the very weak chevron case, and as in I, the chevron growth toward its equilibrium shape is monotonic.

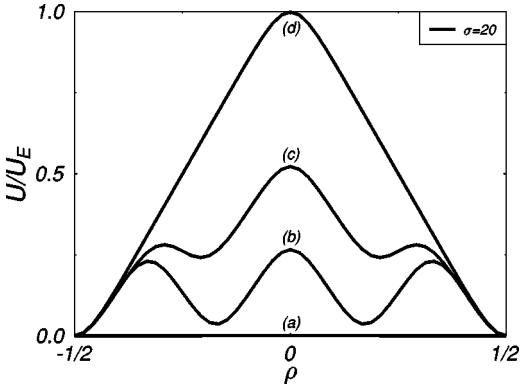

FIG. 6. Time development of the $\sigma=20$ chevron, showing the time dependence of displacement U. Graph legend as in previous figures. Note the transient but now relatively long lasting development of the $n=3$ mode.

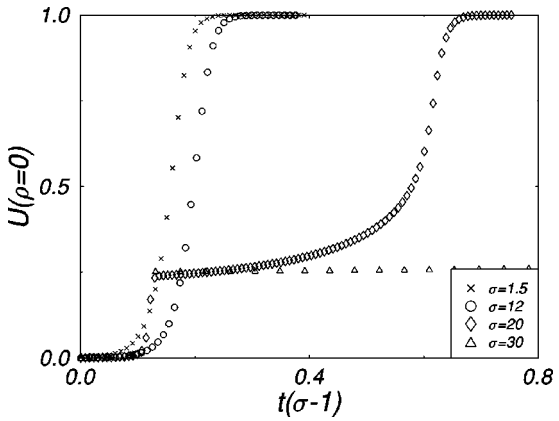

FIG. 7. Time dependence of the normalized displacement $U(0)$ at the midpoint of the cell for various different σ, as discussed in the text. This figure highlights the emergence of new features in the evolution at intermediate (scaled) times for higher σ.

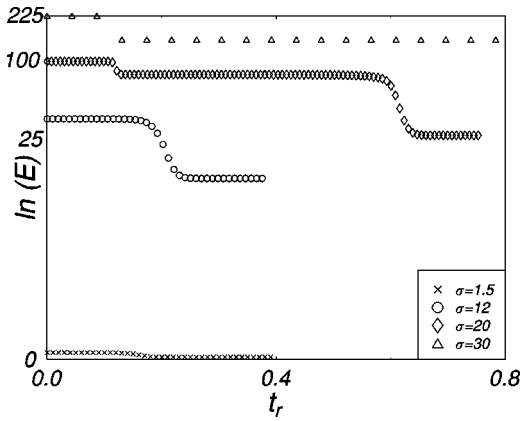

FIG. 9. The time dependence of dimensionless free energy, showing the rapid glitches corresponding to interface annihilation, as discussed in the text. Note the logarithmic energy scale, which disguises the equal magnitude of each energy slippage in nondimensionalized units. The time scale $t_r = t(\sigma - 1)$.

In Figs. 4 and 5 we show analogous graphs for $\sigma = 12$. We recall from Eq. (39) that for this value of σ, the fastest growing mode is the $n = 2$ mode. The influence of the $n = 2$ mode can be discerned in these figures, causing a slightly wobbly chevron shape at intermediate times in Fig. 3. The angular plot exposes this behavior more easily; oscillations in ϑ with wave number 2 are visible at intermediate times. However, the counterpart of the rapid growth of these modes at early times is their rapid disappearance at later times. This occurs here, leading to a late-time conventional chevron, with ϑ now saturated over most of the cell width, with a relatively narrow chevron tip and with healing regions close to the cell walls, as expected.

In Fig. 6 we show the evolution of the layer displacement only for $\sigma = 20$. Here the $n = 3$ mode has the fastest growth, and indeed at intermediate times the displacements form a W shape corresponding to this mode. In this structure there are several (quasi-equilibrium) regions of $\vartheta \approx \pm 1$ separated by chevron-tip structures. At early times (not shown), the multitip structure has not yet developed, and only the fundamental mode grows. This is then overwhelmed by the W structure, which then decays at late times to yield the equilibrium V-shaped chevron structure which possesses only two regions with $\vartheta = \pm 1$.

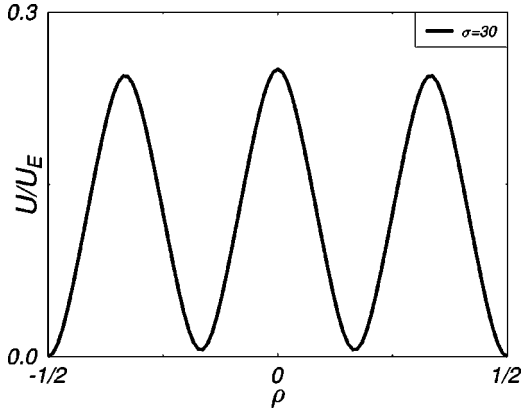

FIG. 8. Metastable $\sigma = 30$ W structure, showing the shape of the well developed $n = 3$ transient found in Fig. 6. Note that although the $n = 4$ transient should grow most quickly at this value of σ, it does not in fact dominate, because nonlinear effects delay its nucleation.

Other aspects of these behaviors are shown in ensuing figures. In Fig. 7 we show the time dependence of the displacement at the midpoint of the cell for several different σ. In order to obtain strictly comparable pictures, we choose runs for which the relative displacement increases at early times at exactly the same speed with respect to the scaled time. The development of higher harmonics is signaled by sharp changes in the time evolution of the displacement at this point.

We see that for $\sigma = 1.5$ the evolution of U is straightforward and monotonic, consistent with Figs. 2 and 3. For $\sigma = 10$, U increases monotonically and thus normally, though the $\sigma = 10$ curve lags behind the $\sigma = 1.5$ curve. This is consistent with the normal time dependence of the growing chevron, but with the transient $n = 2$ wobble, expected from Figs. 4 and 5. By contrast, at $\sigma = 20$ the lag has developed dramatically. The curve more or less stops for a long time while the $n = 3$ structure rapidly develops (Fig. 6), after it has been induced nonlinearly by the $n = 1$ mode. At long times it disappears again with a rather rapid time constant, as the equilibrium structure overwhelms it. For $\sigma = 30$, where the $n = 4$ mode dominates, U seems to settle down to a metastable equilibrium, shown in Fig. 8. This is a metastable $n = 4$ W structure. Similar plots can be drawn for angular features of the time evolution.

Then in Fig. 9, we show the time dependence of the scaled free energies with increasing σ. For $\sigma = 1.5$ the decay is steady. For higher values of σ, the relaxation occurs through a number of rather sharp glitches. These glitches occur when two neighboring chevron tips or, equivalently, $+/-$ wall structures annihilate, thus rapidly reducing the free energy of the system. The final chevron equilibrium is a state dominated by the $n = 1$ harmonic. Each annihilation reduces the dominant mode by one. The idea of interface annihilation will be important and we shall return to it in our comments in the final section on the physical structure of the whole phenomenon.

IV. INTERPRETATION

In order to interpret the results we have reached in this section, it will be necessary also to cast our minds back to the hydrodynamical relaxation discussed in I. This problem involves the relaxation of a layer variable $u(x,t)$, which is a proxy for the phase variable W. The dynamics couples this variable with the hydrodynamic velocity $\mathbf{v}$. The system may be regarded as incompressible, which gives rise to the condition that $\nabla\cdot\mathbf{v}=0$. This condition arises as a result of conservation of matter; if the fluid is incompressible, the divergence-free condition on $\mathbf{v}$ articulates the condition that the fluid outflow from any region exactly balances the inflow.

Interestingly, however, the layer displacement variable u is also a conserved variable. This is essentially because the free energy is not concerned with the value of u itself, but rather its gradient. Then changes in u are simply governed by a conservation law, and it is the analogous current which responds to changes in the gradient of u. The equations (18,19) that articulate these intuitions are but one example of a whole set of coupled order parameter/hydrodynamical equations appropriate to different physical circumstances, which have been adumbrated by Hohenberg and Halperin [12].

In that article these authors listed a whole set of models that have come to be known simply as Models $A,B,\ldots.$, etc. It will be useful to recall from this list the physical significance of the first two. Model A concerned simple relaxation of a nonconserved order parameter, in the absence of hydrodynamic coupling. This model is sometimes known as the Cahn-Allen [13] or simply as the time-dependent Ginzburg-Landau model. In this model an order parameter relaxes to equilibrium with a velocity proportional to the functional derivative of the governing free energy with respect to that order parameter. In model B, or the Cahn-Hilliard model [14,15], there is still no hydrodynamic coupling, but now the order parameter is conserved. The paradigm for such behavior is the relaxation of concentration fluctuations in a binary mixture, in which case clearly material of either species cannot be destroyed. The dynamics is affected by the conservation law, and now the relaxation to equilibrium is proportional not to the functional derivative of the governing free energy with respect to that order parameter itself, but rather to its second gradient.

Model A relaxation is relatively straightforward, and proceeds, roughly speaking, to the nearest equilibrium. In the case of model B, however, domain formation is rife in the early stages. This stage involves rapid relaxation to regions of local equilibria, separated from each other by interfaces. Only in the late stages do the domains coalesce as the interfaces meet each other and mutually annihilate. The late stages can take a very long time indeed.

Returning to the specific problem of this paper, the useful mathematical variable has not been u, but rather ϑ, the layer slope. This is zero in the pure bookshelf geometry, and in equilibrium is either plus or minus some equilibrium value. The free energy has some analogy to the classical Ising model, in which a magnetization takes a nonzero value — either plus or minus — in some control parameter regime. The equations of our problem in ϑ turn out to be model A (in the case discussed in I) and model B (the case discussed here). This may seem counterintuitive. For in I, we *included* hydrodynamic coupling, and finished with simple relaxation; by contrast here, we *omit* it, and find an effective conserved variable.

In any event, although we do not have a good intuitive explanation of why exactly these two cases turn out the way that they do, the dynamics that we find in I involves simple relaxation, and this is consistent with what is expected from model A behavior. By contrast, in this study it is as though we had a binary fluid mixture with two equilibria at concentrations α and β corresponding to $\vartheta=\pm1$. Locally, ϑ is a conserved variable. This slows down the relaxation and leads to the formation of domains. In our case the domains are regions of opposite ϑ, and the interfaces between them correspond to the cusps of the W structures we have found. Indeed the quasi-equilibria are sufficiently stable to slow down the equilibration process to time scales longer than we are able to observe them.

V. CHEVRON PHASE INVASION

In the preceding sections we have studied the chevron formation taking the process to be homogeneous within the cell — so-called homogeneous nucleation. By analogy with other nucleation processes, however, we might alternatively suppose that the original bookshelf structure suffers from spontaneous chevronlike defects that serve as nucleation centers for the chevron structure when $\sigma\geqslant1$. In this case we would expect the chevron formation not to occur as an essentially homogeneous process, but rather by an invasion. A front between the chevron and bookshelf regions, initially close to the spontaneous defect, would then advance into the bookshelf region until the chevron deformation filled the whole system. In this section we model this possibility.

We first derive the nonlinear dynamical equation governing displacement $u(x,z,t)$. We shall then use it to study permeation waves traveling in the z direction. The fundamental equation follows from substituting Eq. (4) into Eq. (20):

$$u_t=-\lambda_p B\left[\left(\frac{\partial}{\partial z}-\frac{\partial}{\partial x}u_x\right)\left(\frac{1}{2}u_x^2-u_z-\epsilon\right)+\frac{L^2}{4\pi^2}\epsilon_c u_{xxxx}\right]. \tag{42}$$

In order to simplify the discussion, we consider only strains in the near-critical regime. By analogy with Eq. (13) we adopt the ansatz

$$u(x,z,t)=\frac{L}{2\pi}A(z,t)[1+\cos(2\pi x/L)]. \tag{43}$$

The quantity $A(z,t)=A_{\mathrm{eq}}g(z,t)$ with A_{eq} the amplitude of the fundamental mode, whose static properties we have examined in Sec. II B. In particular, we have observed that close to the cell edge A changes on length scale ξ_p defined in Eq. (16).

The projection of Eq. (43) onto the fundamental mode yields the time-dependent generalization of Eq. (15), which is also the space-dependent version of Eq. (40):

$$\frac{3}{4\pi^2(\sigma-1)}\tau_p\frac{\partial g}{\partial t}=\xi_p^2\frac{\partial^2 g}{\partial z^2}+g-g^3. \tag{44}$$

We can now rescale time and space variables:

$$\tilde{t}'=\frac{4\pi^2(\sigma-1)}{3\tau_p}t, \quad \tilde{z}=\frac{z}{\xi_p}. \tag{45}$$

The fundamental time scale $\tilde{t}'$ differs from $\tilde{t}$ by a factor depending on the chevron number σ. The length ξ_p defined by Eq. (16) also depends on σ. In both cases the rescaling takes into account critical effects so that the fundamental time and spatial scales, although set by microscopic quantities, diverge as the critical point $\sigma=1$ is approached.

In the scaled variables Eq. (44) is now the well known modified Fisher or Fisher-Kolmogorov equation [16]:

$$\frac{\partial g}{\partial \tilde{t}'}=\frac{\partial^2 g}{\partial \tilde{z}^2}+g(1-g^2). \tag{46}$$

This equation is a paradigm for the analysis of systems that are suddenly quenched into an unstable state, and whose subsequent time evolution is dominated by domain wall propagation. Let us summarize its properties.

The state $g=0$ is unstable, whereas the states $g=\pm 1$ are stable. Depending on the initial conditions, chevron structure formation may occur either by uniform growth (which we have discussed in Sec. III C) or by domain wall propagation. The properties of the domain walls in this and related models have been discussed extensively in the literature [17–21]. This domain wall lies between the unstable state $g=0$ and the stable state $g=\pm 1$, and advances into the $g=0$ region. The net result is the replacement of the $g=0$ region by a $g=\pm 1$ regime.

The Fisher-Kolmogorov equation (46) sustains many domain wall solutions with different velocities. A particularly simple tanh solution [22], which has been discovered on a number of different occasions, is

$$g=\frac{\exp[3/2\,(\tilde{t}'-\tilde{t}_0')-(1/\sqrt{2})\tilde{z}]}{1+\exp[3/2\,(\tilde{t}'-\tilde{t}_0')-(1/\sqrt{2})\tilde{z}]}. \tag{47}$$

This solution describes the advance of the wall dividing the chevron structure from the bookshelf structure. The wall moves into the bookshelf structure with speed $3/\sqrt{2}$ and characteristic width $\sqrt{2}$ in dimensionless units.

However, this solution is not unique. There are exact domain wall solutions of the form $A(\tilde{t}',\tilde{z})=g(\tilde{z}-v\tilde{t}')$ traveling with arbitrary velocities $v\geqslant v_c$ [23], where v_c is the so-called marginal stability velocity.

However, Aronson and Weinberger [22] have shown that for the (rather natural) initial condition that $A(\tilde{z},\tilde{t}'=0)$ decays faster than $e^{-\tilde{z}}$ for large $\tilde{z}$, the domain wall velocity approaches the marginal stability velocity $v_c=2$. The marginal stability criterion and its clear physical interpretation has been given by Dee and Langer [23]. A detailed study of the Fisher-Kolmogorov equation in physical terms has been carried out by Saarloos [16]. Some experimental studies of these traveling waves in a liquid crystal context can be found in [24,25].

Thus, nothwithstanding the multiplicity of the solution manifold, in practice both numerical and physical domain walls are expected to travel at the velocity $v_c=2$.

Retranslating the nondimensional $\tilde{z}$ and $\tilde{t}$ into physical variables using Eq. (45), we find that the nondimensional velocity $v_c=2$ corresponds to physical velocity:

$$v_{\rm wall}=\frac{4\pi B\lambda_p}{L}\left(\frac{\epsilon-\epsilon_c}{3}\right)^{1/2}v_c. \tag{48}$$

A numerical estimate of $v_{\rm wall}$, taking $\epsilon=10^{-6}$, $L=10^{-3}$ cm, and $B\lambda_p=10^{-5}$ cm^2 s^{-1} [8] yields $v_{\rm wall}\sim 10^{-4}$ cm s^{-1}. The physical width of the wall is $\sim\xi_p$.

We have also carried out some unsystematic but revealing simulations of the late stages of domain-wall driven nucleation. We find that if a bookshelf region is invaded from the left by a $g=+1$ chevron region and from the right by a $g=-1$ region (or vice versa), then the domain walls collide when the bookshelf region is completely overwhelmed. The collision process leaves behind, on a time scale $\sim\tau_p'=\tau_p/(\sigma-1)$, a stationary $-1/+1$ wall of width $\sim\xi_p$. This domain wall is closely analogous to the healing region close to the cell edge discussed in Sec. II B. Similarly, if the bookshelf region is invaded from both sides by chevron regions with the same polarity, then domain-wall collision leads to a homogeneous static chevron region. The memory of the collision disappears over a time scale τ_p'. If, however, a small (one-dimensional) $g=-1$ region is trapped within two larger $g=+1$ regions, then the inside $g=-1$ region is destroyed on rather long time scales. Equivalently, the $-1/+1$ domain walls attract weakly. We have not, however, carried out detailed studies of this process.

VI. SUMMARY AND CONCLUSIONS

In this paper we have continued the study of the dynamics of chevron formation in a Sm-*A* phase following a quench of a bookshelf structure into an unstable state. The dynamical equations are derived from the standard formulations of Sm-*A* liquid crystal hydrodynamics, although this set of papers is, to our knowledge, their first application in this context.

This equilibrium chevron phase results from the mismatch between the layer spacings in the bulk and at the interfaces. Our free energy is closely related to that used by one of us earlier in a study of the statics [6], and also to that used by Limat and Prost [5] in an analogous study.

The dynamics is strongly dependent on the conditions at the edges of the cell. In principle, there is strong coupling between layer relaxation and hydrodynamic flow. We have found in paper I of this series that it is the hydrodynamic flow which is normally expected to play the major role in the dynamics of the layer distortion. In this subsequent paper we have shown that when mass flow is forbidden by the cell edge conditions, the dynamics of the formation of the chevron structure occurs by layer permeation. In this process, the layer structure diffuses through the stationary fluid.

This process is governed by the nonlinear modified Fisher

equation and is extremely slow. Even in the case of a very thin cell, $L=10^{-3}$ cm, it can take several hours. In principle, the chevron phase may form uniformly over the whole sample, or it may be nucleated from a chevronlike defect in the initial bookshelf structure. In the latter case the invasion front is extremely slow: $v\sim 10^{-4}$ cm s^{-1}. At this stage it is difficult to make a definite prediction between these two scenarios.

However, the most striking prediction concerns uniform chevron formation. We have shown that when hydrodynamical interactions dominate, the chevron formation is monotonic and is akin to the relaxation of any nonconserved order parameter; it exhibits model *A* behavior. The amplitude of the chevron grows in time starting from an initial fluctuation. In that case, in some sense, the chevron formation is not only monotonic, but also monotonous.

If the hydrodynamical interaction is disrupted, however, as discussed in this paper, not only is the chevron formation many orders of magnitude slower, but its qualitative nature changes for sufficiently deep quenches. Now the relaxation is as though the angular variable were conserved and it exhibits model *B* behavior. For shallow quenches to moderate chevron numbers $\sigma\leqslant 5$, the chevrons grow steadily toward the conventional V shape; no surprises there. For higher σ, by contrast, it seems that there are remarkable long-lasting quasi-metastable intermediate W-like structures. We speculate that very slight cell defects might stabilize these multichevron-tip structures.

Finally, this work raises a number of interesting questions to which we hope to return in further research. First, our condition of zero flow with fixed edges is clearly an idealization. We anticipate that a more detailed study of the hydrodynamics would yield a perturbation structure, with flow induced by a coupling parameter $\delta_2=\tau_v/\tau_p\sim 10^{-8}$, and with the possibility of compressibility effects playing a nonnegligible role. Second, the extension of this kind of process to the Sm-*C* phase, in which there are extra orientational degrees of freedom, may or may not be straightforward.

ACKNOWLEDGMENTS

A.N.S. is grateful to EPSRC and INTAS for financial support in Southampton and St. Petersburg. L.D.H. is grateful to EPSRC and DERA, Malvern for their financial support. We are grateful to E. I. Kats, S. Kralj, N. Vaupotič, S. Žumer, and A. A. Wheeler for useful discussions.

[1] A. N. Shalaginov, L. D. Hazelwood, and T. J. Sluckin, Phys. Rev. E **58**, 7455 (1998).
[2] T. P. Rieker, N. A. Clark, G. S. Smith, D. S. Parmar, E. B. Sirota, and C. R. Safinya, Phys. Rev. Lett. **59**, 2658 (1987).
[3] Y. Takanishi, Y. Ouchi, H. Takezoe, and A. Fukuda, Jpn. J. Appl. Phys., Part 2 **28**, L487 (1989).
[4] Y. Ouchi, Y. Takanishi, H. Takazoe, and A. Fukuda, Jpn. J. Appl. Phys., Part 1 **28**, 2547 (1989).
[5] L. Limat and J. Prost, Liq. Cryst. **13**, 101 (1993).
[6] S. Kralj and T. J. Sluckin, Phys. Rev. E **50**, 2940 (1994).
[7] M. Nakagawa and T. Akahane, J. Phys. Soc. Jpn. **55**, 1516 (1986).
[8] P. G. de Gennes and J. Prost, *The Physics of Liquid Crystals* (Clarendon Press, Oxford, 1993).
[9] E. I. Kats and V. V. Lebedev, *Fluctuation Effects in the Dynamics of Liquid Crystals* (Springer-Verlag, Berlin, 1994).
[10] M. Delaye and P. Keller, Phys. Rev. Lett. **37**, 1065 (1976).
[11] D. Zwillinger, *Handbook of Differential Equations* (Academic, London, 1992).
[12] P. C. Hohenberg and B. I. Halperin, Rev. Mod. Phys. **49**, 435 (1977).
[13] S. M. Allen and J. W. Cahn, Acta Metall. Mater. **27**, 1085 (1979).
[14] J. W. Cahn and J. E. Hilliard, J. Chem. Phys. **28**, 258 (1958).
[15] J. W. Cahn, Trans. Metall. Soc. AIME **242**, 166 (1968).
[16] See, e.g., W. van Saarloos, Phys. Rev. A **37**, 211 (1988); **39**, 6367 (1989). and R. A. Fisher, Ann. Eugenics **7**, 355 (1937). See I for a further discussion of this equation. Note also that although this equation also crops up in I, it occurs in an entirely different context, that of *hydrodynamically driven homogeneous* chevron formation, rather than *permeation-driven inhomogeneous* chevron formation.
[17] J. D. Gunton, M. San Miguel and P. S. Sahni, in *Phase Transitions and Critical Phenomena*, edited by C. Domb and J. L. Lebowitz (Academic, New York, 1983), Vol. 8, p. 267.
[18] K. Binder, Rep. Prog. Phys. **50**, 783 (1987).
[19] See, e.g., *Homogeneous Nucleation Theory*, edited by F. F. Abraham (Academic, New York, 1974).
[20] J. B. Collins and H. Levine, Phys. Rev. B **31**, 6119 (1985).
[21] S. A. Schofield and D. W. Oxtoby, J. Chem. Phys. **94**, 2176 (1991); H. Löwen, S. A. Schofield, and D. W. Oxtoby, J. Chem. Phys. **94**, 5685 (1991).
[22] D. G. Aronson and H. F. Weinberger, *Partial Differential Equations and Related Topics* (Springer, Heidelberg, 1975).
[23] G. Dee and J. S. Langer, Phys. Rev. Lett. **50**, 383 (1983).
[24] Guozhen Zhu, Phys. Rev. Lett. **49**, 1332 (1992).
[25] J. E. Maclennan, M. A. Handschy, and N. A. Clark, Phys. Rev. A **34**, 3554 (1986).